Peptides and Gd Complexes Containing Colloidal Assemblies as Tumor-Specific Contrast Agents in MRI: Physicochemical Characterization

Mauro Vaccaro,*†‡ Antonella Accardo,§ Gerardino D'Errico,*† Karin Schillén,‡ Aurel Radulescu,¶ Diego Tesauro,§ Giancarlo Morelli,§ and Luigi Paduano*†

*Department of Chemistry, University of Naples "Federico II", Naples, Italy; †CSGI (Consorzio per lo Sviluppo dei Sistemi a Grande Interfase), Florence, Italy; ‡Physical Chemistry 1, Center for Chemistry and Chemical Engineering, Lund University, Lund, Sweden; §Department of Biological Sciences, CIRPeB University of Naples "Federico II", and the National Research Council Institute of Bioimaging and Biostructure (IBB CNR), Naples, Italy; and ¶Jülich Centre for Neutron Science (JCNS), Forschungszentrum Jülich GmbH, Jülich, Germany

ABSTRACT The aggregation behavior of an amphiphilic supramolecular system, with potential application as a tumor-specific magnetic resonance imaging contrast agent, has been studied in detail by dynamic light scattering, small-angle neutron scattering and cryotransmission electron microscopy. The system was constituted of mixed aggregates formed by an anionic unimer containing the DTPAGlu, a chelating agent for the paramagnetic Gd^{3+} ion, and an uncharged unimer containing the bioactive peptide CCK8, capable of directing the assembly toward tumor cells. Mixed aggregates formed by both unimers, and in the case of the DTPAGlu unimer with the chelating agent as free base or as Gd^{3+} complex, have been investigated. A number of interesting features of the aggregation behavior were revealed: at physiological pH, micelles and bilayer structures were present, whereas upon decreasing solution pH or increasing ionic strength, the formation of bilayer structures was favored. On the basis of the above observations, the aggregating mechanism has been elucidated by considering the screening effect on intra- and interaggregate electrostatic repulsions.

INTRODUCTION

During the last years, medical MRI has become one of the most efficient diagnostic techniques. This progress has been largely supported by the use of contrast agents that improve the contrast and have highly resolved images. Currently, ~30% of all MRI images are obtained using contrast agents, and this use is increasing (1).

In general, the contrast comes from local differences in spin relaxation time along longitudinal (T_1) and transverse (T_2) planes of the main magnetic field applied to the specimen.

In current medical diagnostics, the most frequently used contrast agents are T_1 agents, and among these, due to its high number of unpaired electrons, the Gd^{3+}, in its complexed form Gd-DTPA (Gd-diethylenetriaminepentaacetate, commercial name Magnevist), is the most diffused.

The Gd^{3+} enhances MRI contrast by shortening the longitudinal relaxation time of the water protons present in its coordination sphere. This is generally expressed as proton relaxivity (r_1), which defines the increase in longitudinal water proton relaxation rate per millimolar concentration of Gd^{3+}. The relaxivity might be theoretically increased to >100 mM^{-1} s^{-1} for monohydrated chelates compared to 4.5 mM^{-1} s^{-1} of the Gd-DTPA commercial complex when electron-spin relaxation, water exchange, and rotation are simultaneously optimized. Namely, the electron-spin relaxation, is difficult to modify on a rational basis. Tuning the water exchange rate to the optimal value ($k_{ex} = 10^8$ s^{-1}) is also problematic (2). Thus, the most modifiable factor is the rotation of the complex, which has to be slow enough to enhance the relaxivity value. Commonly, this has been achieved by assembling gadolinium complexes with macromolecules. With this aim, numerous potential contrast agents have been proposed, including dendrimers (2), polymers (3), proteins (4), water-gadofullerenes (5), and supramolecular amphiphilic aggregates such as micelles (6) and liposomes (7).

In most of the above systems, the contrast agents were designed to enhance their half-life in blood, and to improve their tissue perfusion or excretion (8) and their relaxivity value. None of the proposed systems has been accomplished with a view to increasing specificity. In fact, an ideal MRI contrast agent should increase the signal intensity at the target site and at the same time lower the signal intensity in the vascular space, thus eliminating the disadvantageous value of the background.

Some attempts to attain tumor-specific MRI contrast agents have been made using the pH (9) or enzymatic activity (10)

Submitted March 14, 2007, and accepted for publication April 24, 2007.

Address reprint requests to Luigi Paduano, Dept. of Chemistry, University of Naples "Federico II", Via Cynthia, 80126 Naples, Italy. E-mail: luigi.paduano@unina.it.

Abbreviations used: MRI, magnetic resonance imaging; CCK, cholecystokinin; CCK8, C-terminal octapeptide of cholecystokinin; CCK_A-R and CCK_B-R, cholecystokinin receptor types A and B; cmc, critical micellar concentration; DTPAGlu, N,N-bis[2-[bis(carboxy-ethyl)amino]ethyl]-L-glutamic acid; FT-PGSE-NMR, Fourier transformed, pulsed-gradient spin-echo nuclear magnetic resonance; SANS, small-angle neutron scattering; DLS, dynamic light scattering; cryo-TEM, cryogenic transmission electron microscopy.

Editor: Jill Trewhella.

0006-3495/07/09/1736/11 $2.00

doi: 10.1529/biophysj.107.107417

at the tumor site. However, studies reveal that the pH of the tumor site may differ from person to person, and in the latter case, a model enzyme was used, not a tumor-specific enzyme. More promising, it seems, would be the use of a bioactive molecule, such as a peptide or an antibody, capable of delivering the active principles to target cells.

In recent years, with the aim of increasing the relaxivity and specificity of contrast agents, we have proposed mixed amphiphilic aggregates containing a derivative of DTPAGlu (polydentate chelating agent for the Gd^{3+}) and the bioactive peptide CCK8, able to target the cell assembly. The first unimer is constituted by an alkylic moiety bound, through a lysine residue, to the DTPAGlu (11). The second contains the same alkylic moiety bound, through an oxyethylene glycol spacer, to the C-terminal cholecystokinin octapeptide amide (CCK 26–33 or CCK8) (12).

The choice of the CCK8 peptide is based on the knowledge that this peptide displays high affinity for both membrane cholecystokinin receptors, CCK_A-R and CCK_B-R (13). Both CCK_A-R and CCK_B-R are very consolidated targets due to their overexpression in many tumors: CCK_A-R is overexpressed in pancreatic cancer, and CCK_B-R is found in small-cell lung cancer, colon and gastric cancers, medullary thyroid carcinomas, astrocytomas, and stromal ovarian tumors (14).

A first attempt was carried out with single-tailed molecules that self-assemble in spherical micelles (6). Although the relaxivity values measured on these were very encouraging (17.5 mM^{-1} s^{-1} for the binary system and 18.7 mM^{-1} s^{-1} for the mixed system), the large number of free unimers (cmc $\sim 10^{-5}$ mol kg^{-1}) present in the system was judged unsuitable for medical purposes. Furthermore, the length of the oxyethylene glycol spacer in the peptide unimer was not found to guarantee an efficient exposure of the CCK8 beyond the aggregate surface.

Thus, to form micelles with significantly lower cmc values ($\sim 10^{-7}$ mol kg^{-1}) and long-lived aggregates such as bilayer structures, we have redesigned the molecules with a double C18 alkyl tail. Recently, we presented a detailed characterization of only the aggregates formed by the double-tailed DTPAGlu unimer (15). Here, we extend the characterization to the mixed supramolecular aggregates in which a selective agent has been added. We have carried out several attempts to optimize the design of the CCK8 unimer, varying the length of the spacer situated between the double tail and the CCK8. In fact, the spacer should be long enough to assure an efficient exposure of the peptide on the surface of the aggregate, as mentioned above, and at the same time short enough to favor vesicle formation (16). Therefore, we have studied the systems containing the supramolecular aggregates $(C18)_2$DTPAGlu-$(C18)_2$L5CCK8 and $(C18)_2$DTPAGlu(Gd)-$(C18)_2$L5CCK8, in which the spacer (L5) consists of 5 units of 8-amino-3,6-dioxaoctanoic acid, and we recently reported the relaxometric characterization of Gd^{3+} containing mixed aggregates (17). In this article, we present a detailed physicochemical characterization of these supramolecular aggregates; the effect on aggregation behavior with respect to pH and ionic strength also has been investigated, due to the variety of environmental conditions the contrast agents experience.

EXPERIMENTAL

Materials

The surfactants used in this work, $(C18)_2$DTPAGlu or its gadolinium complex $(C18)_2$DTPAGlu(Gd) and $(C18)_2$L5CCK8 (Fig. 1), were synthesized in solid phase under standard conditions using Fmoc strategy, as reported elsewhere (17). All other chemicals were commercially available from Sigma Aldrich (St. Louis, MO), Fluka (Buchs, Switzerland), or LabScan (Stillorgan, Dublin, Ireland) and were used as received unless otherwise stated. All solutions were prepared by weight with doubly distilled water. Samples to be measured by the FT-PGSE-NMR and SANS techniques were prepared using heavy water (Sigma Aldrich, purity >99.8%).

Sample preparation

All solutions were prepared by weight, buffering the samples at a defined pH value in the 3.0–7.4 range. Two different buffer solutions were used: a 0.10 M phosphate buffer for pH 7.4 and a 0.10 M citric acid/phosphate buffer for lower pH values. pH measurements were made using pH-meter MeterLab PHM 220. The samples were prepared by dissolving the unimers in a small amount of an organic solvent (methanol/chloroform = 50:50 mixture), and subsequently evaporating the solvent by slowly rotating the tube containing the solution under a stream of nitrogen. In this way, a thin film of amphiphile was formed. After leaving the film under reduced pressure for several hours, the organic solvent was evaporated. The film was then hydrated by adding the buffer solution in the vial and stirred for 1 h by vortex. The product

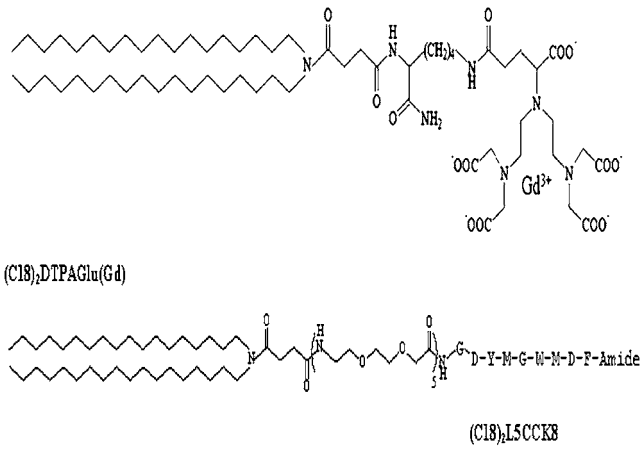

FIGURE 1 Schematic representation of the $(C18)_2$DTPAGlu(Gd) and $(C18)_2$L5CCK8 unimers employed to formulate aggregates.

successively underwent sonication for 3–4 h to yield small and multilamellar vesicles, and finally was extruded 11 times through a polycarbonate membrane with 100-nm pore size to obtain large and unilamellar vesicles. Aggregate solutions containing NaCl (0.9 wt %) were prepared in a similar way. In all cases, for ternary systems, the imposed molar ratio chosen between the two solutes, $(C18)_2$DTPAGlu (or its gadolinium complex $(C18)_2$DTPAGlu(Gd)) and $(C18)_2$L5CCK8, was 70:30.

Self-diffusion measurements

PGSE-FT ^{1}H NMR experiments for determination of self-diffusion coefficients were performed on a 600 MHz Bruker Avance spectrometer (Bruker, Madison, WI). ^{1}H NMR diffusion measurements were performed using a stimulated echo sequence with bipolar gradient pulses (18). For a system of monodisperse diffusing particles, the normalized PGSE-NMR echo signal, I, is given by:

$$I(k) = \exp(-kD), \tag{1}$$

where $k = \gamma^2 g^2 \delta^2 (\Delta - \delta/3)$. γ is the magnetogyric ratio of the proton, δ is the duration of the field-gradient pulses, and Δ, the diffusion time, is the distance between the leading edges of the gradient pulses. In this work, echo delays were kept constant so that the relaxation effect would not be accounted for; diffusion time was set to 100 ms and the pulsed gradients, with a duration of 8 ms, were incremented from 2% to 95% of the maximum strength in 16 spaced steps. The sample temperature was controlled at 25.1 ± 0.1°C during measurements by passage of controlled-temperature air through the sample holder.

Dynamic light scattering

The setup for the dynamic light scattering measurement was an ALV/DLS/SLS-5000F, CGF-8F based compact goniometer system (ALV-GmbH, Langen, Germany). The light source was constituted by a CW diode-pumped Nd:YAG solid-state Compass-DPSS laser with a symmetrizer from Coherent(Santa Clara, CA). It operated at 532 nm with a fixed output power of 400 mW. The laser intensity could be modulated by an external compensated attenuator from Newport (Irvine, CA). A more detailed description about the instrumentation can be found in the literature, with the difference that *cis*-decahydronaphtalene was used instead of toluene as a refractive index matching liquid (19).

Small-angle neutron scattering

SANS measurements were performed at the V4 facility of the Hahn and Meitner-Institut, Berlin, Germany, and at the KWS2 instrument located at the FRJ-2 reactor of the Forschungszentrum of Jülich. In the first case, a neutron beam of $\lambda = 7$ Å with a spread $\Delta\lambda/\lambda = 0.1$ was used. A 2D detector allowed the collection of data in an interval of transferred moment q ranging between 0.003 and 0.15 Å^{-1}. In the latter case, neutrons with an average wavelength λ of 6.2 Å and a wavelength spread $\Delta\lambda/\lambda < 0.1$ were used. A two-dimensional array detector at three different sample-to-detector distances, 2, 8, and 20 m, detected neutrons scattered from the samples. These configurations allowed measurement of the scattered intensity in a range of the transferred moment q between 0.002 and 0.18 Å^{-1}. The measurement time ranged between 30 and 120 min per sample.

The obtained raw data were corrected for electronic background and empty cell scattering. Detector sensitivity corrections and transformation to absolute scattering cross sections $d\Sigma/d\Omega(q)$ were made with a secondary Plexiglass standard according to the equation

$$\frac{d\Sigma}{d\Omega}(q) = \left(\frac{d\Sigma}{d\Omega}\right)_P \frac{d_P T_P L_S^2}{d_S T_S L_P^2 I_P}[(I_S - I_{bck}) - T_S(I_{EC} - I_{bck})], \tag{2}$$

where subscripts P and S are for Plexiglass and sample, respectively. The cell thicknesses and transmissions are indicated by d and T, respectively, whereas L_S and L_P are detector distances at which sample and Plexiglass were measured to get I_S and I_P. Raw data were also corrected for intensities of background, I_{bck}, and empty cell, I_{EC}. Finally, data were radially averaged and absolute scattering cross sections were obtained.

Cryogenic transmission electron microscopy

Cryo-TEM is a suitable technique for the direct visualization of surfactant aggregates ranging in size from ~5–10 nm to 1 μm. The samples were prepared and transferred according to the usual procedure. The sample was placed in the controlled environment vitrification chamber at room temperature, to avoid water evaporation and to ensure cryofixation of the specimen at 25°C (20). A 5-μL drop of the sample solution was applied on a copper electron microscopy grid with a holey carbon film, and excess solution was blotted with a filter paper, to create a thin sample film spanning the holes in the carbon film. Then the grid was rapidly plunged into liquid ethane at its melting temperature. The vitrified specimen was then transferred under liquid nitrogen environment by use of a cold stage unit into the electron microscope. A Philips CM120 BioTWIN Cryo electron microscope operating at 120 kV was used.

RESULTS

Self-diffusion

The self-diffusion coefficients were measured for the $(C18)_2$DTPAGlu-water, $(C18)_2$L5CCK8-water binary systems,

and for the $(C18)_2$DTPAGlu-$(C18)_2$L5CCK8-water ternary system. For each system, the total solute molality was 100 times greater than the corresponding cmc values (17). Under these conditions, the unimeric species contributions are negligible, and only the amphiphilic molecules present in the aggregates are responsible for measured self-diffusion coefficients. Because of the line broadening due to the paramagnetic ion, no self-diffusion measurements could be performed on the systems containing $(C18)_2$DTPAGlu unimer as Gd complex. In the ternary system, the DOSY experimental evidence indicates that the solutes present in solution form mixed aggregates and diffuse together. The experimental self-diffusion coefficients, D, are collected in Table 1. In the approximation of very diluted solution the data can be directly related to the hydrodynamic radii (see Table 1) of the aggregates, R_H, through the Stokes-Einstein equation, which holds for noninteracting hard spheres diffusing in a continuous medium:

$$R_H = \frac{k_B T}{6\pi\eta D}, \tag{3}$$

where k_B is the Boltzmann constant, T the absolute temperature, and η the medium viscosity. Inspection of Table 1 shows that in all cases R_H is clearly larger than what is reasonable for spherical aggregates (21). This means that some of the assumptions on which Eq 3 is based are not valid, i.e., strong intermicellar interactions are present, or the micelle shape is far from spherical.

Binary systems: $(C18)_2$DTPAGlu-water and $(C18)_2$L5CCK8-water

In aqueous solution, $(C18)_2$DTPAGlu micelles present a self-diffusion coefficient that is significantly lower than that measured for the single-tailed analog. In fact, although C18DTPAGlu forms spherical micelles with a relatively small hydrodynamic radius (37 Å), the high R_H value obtained for $(C18)_2$DTPAGlu is not compatible with the spherical shape (15). $(C18)_2$L5CCK8-water forms micelles with a D lower than that obtained for $(C18)_2$DTPAGlu, and, consequently, a higher R_H value.

Ternary system: $(C18)_2$DTPAGlu-$(C18)_2$L5CCK8-water

Self-diffusion measurements indicate that $(C18)_2$DTPAGlu-$(C18)_2$L5CCK8 mixed aggregates present hydrodynamic dimensions similar to those of $(C18)_2$DTPAGlu pure aggregates.

TABLE 1 Diffusion coefficients and hydrodynamic radii obtained from PGSE-NMR measurements for the pure and mixed systems studied

Systems	$D \times 10^9$ (m^2s^{-1})	R_H (Å)
$(C18)_2$DTPAGlu (0.00035 mol kg^{-1})	0.032 ± 0.005	63 ± 10
$(C18)_2$L5CCK8 (0.00033 mol kg^{-1})	0.025 ± 0.003	80 ± 15
$(C18)_2$DTPAGlu (0.00032 mol kg^{-1})-$(C18)_2$L5CCK8 (0.00012 mol kg^{-1})-D_2O	0.035 ± 0.002	57 ± 10

DLS

DLS measurements were made on $(C18)_2$DTPAGlu-$(C18)_2$L5CCK8 and $(C18)_2$DTPAGlu(Gd)-$(C18)_2$L5CCK8 aqueous solutions at different scattering angles (θ) ranging from 45° to 140°.

Ternary system: $(C18)_2$DTPAGlu-$(C18)_2$L5CCK8-water

Fig. 2 *a* shows a typical measured intensity correlation (pseudocross) function for the system at 90°. The corresponding

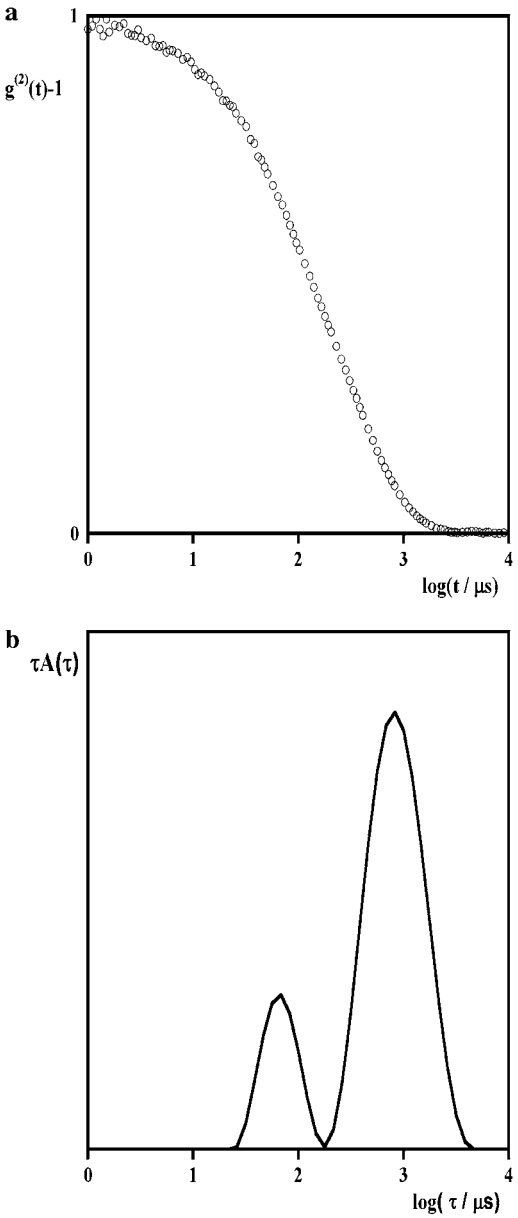

FIGURE 2 (*a*) Intensity correlation function at $\theta = 90°$ for $(C18)_2$DTPAGlu-$(C18)_2$L5CCK8 solution. (*b*) The corresponding relaxation-time distribution obtained from regularized inverse Laplace transformation of the intensity correlation function.

relaxation time distribution [$\tau A(\tau)$ versus $\log(\tau/\mu s)$], obtained by regularized inverse Laplace transformation of the correlation function, is presented in Fig. 2 *b*. The distributions were bimodal at all angles studied and consisted of a small-amplitude fast peak and a large-amplitude slow peak. The apparent size of the aggregates formed in the ternary system was also determined from DLS measurements. In the limit of small scattering vectors, q, the apparent collective diffusion coefficient (D) for a translational process at finite concentration can be calculated from the relaxation rate Γ, which is obtained from the first moment of the translational mode in the relaxation time distribution. D can then be estimated from the slope of Γ, as a function of q^2 (see Eq. 6 in the DLS paragraph of the Appendix). Both modes were found to be diffusive and the values obtained for the fast and slow modes were $D_{fast} = (30.9 \pm 0.9) \times 10^{-12}$ m^2/s and $D_{slow} = (2.9 \pm 0.2) \times 10^{-12}$ m^2/s, respectively (Table 2). The apparent hydrodynamic radii, R_H, were evaluated from these values, using the Stokes-Einstein equation (Eq. 3), as 64 ± 2 and 687 ± 38 Å, for the fast and slow modes respectively. We can conclude from these DLS measurements that two types of aggregate exist in the $(C18)_2$DTPAGlu-$(C18)_2$L5CCK8-water system under the present conditions: micelles and bigger aggregates, such as bilayer structures, as revealed below by SANS results.

Ternary system: $(C18)_2$DTPAGlu(Gd)-$(C18)_2$L5CCK8-water

DLS measurements were also performed on a mixed system in which gadolinium ion was complexed by the chelating agent unimer. The obtained relaxation time distribution was bimodal, as in the gadolinium free case, and was clearly dominated by the slow mode (Fig. 3). The apparent translational diffusion coefficients obtained for the fast and slow modes were $D_{fast} = (33.2 \pm 0.2) \times 10^{-12}$ m^2/s and $D_{slow} = (2.5 \pm 0.3) \times 10^{-12}$ m^2/s, with corresponding R_H values of 61 ± 4 and 810 ± 110 Å (Table 2).

pH effect

The aggregation behavior of the $(C18)_2$DTPAGlu(Gd)-$(C18)_2$L5CCK8 system was also studied by DLS as a function of the pH over a large pH range (pH 7.4–3) because of the increasing importance of pH-sensitive contrast agents. The pH values selected for this study were pH 7.4, which corresponds to physiological pH condition; pH 4.5, because of the pK_a of carboxylic acids; and, finally, pH 3, since the extracellular fluid of tumor cells is acidic. It is observed that the relaxation time distributions clearly vary upon decreasing the pH (Fig. 3), providing an indication of the structural evolution of the aggregates in solution. At pH 7.4, as discussed above, the distribution is bimodal, that is, micelles and bilayer structures are simultaneously present, whereas at pH 4.5, the distribution is dominated by one relaxation mode. Further acidification to pH 3 does not modify significantly the monomodal picture. The low-amplitude peaks at faster times are artifacts that originate either from the inverse Laplace transformation calculation or from the decreased solubility of the sample at low pH values. The linear relation between the relaxation rate and q^2 confirms that the observed single relaxation mode is due to a translational diffusion process attributed to an aggregate that diffuses with a D value of $(2.9 \pm 0.2) \times 10^{-12}$ m^2/s, which corresponds to an R_H value of 669 ± 40 Å (Table 2).

Ionic strength effect

Fig. 4 shows relaxation time distributions obtained from the DLS data at different scattering angles on the $(C18)_2$DTPAGlu(Gd)-$(C18)_2$L5CCK8 aqueous solutions at physiological pH containing sodium chloride, NaCl, at 0.9 wt %, a value corresponding to the physiological ionic strength condition. The relaxation time distributions are monomodal at all angles, showing one broadened peak (data not reported). This mode, which is diffusive, is attributed to

TABLE 2 Parameters obtained by scattering techniques for the systems studied

Systems	pH	$D_{fast} \times 10^{12}$ (m^2 s^{-1})	R_H (Å)	$D_{slow} \times 10^{12}$ (m^2 s^{-1})	R_H (Å)	N*agg*	*R* (Å)	*L* (Å)	*d* (Å)
$(C18)_2$DTPAGlu (0.00030 mol kg^{-1})-$(C18)_2$L5CCK8 (0.00012 mol kg^{-1})-water	7.4	30.9 ± 0.9	64 ± 2	2.9 ± 0.2	687 ± 38	310 ± 60	36 ± 7	262 ± 32	68 ± 9
$(C18)_2$DTPAGlu(Gd) (0.00030 mol kg^{-1})-$(C18)_2$L5CCK8 (0.00013 mol kg^{-1})-water	7.4	33.2 ± 0.2	61 ± 4	2.5 ± 0.3	810 ± 110	270 ± 40	33 ± 5	269 ± 42	53 ± 8
$(C18)_2$DTPAGlu(Gd) (0.00033 mol kg^{-1})-$(C18)_2$L5CCK8 (0.00016 mol kg^{-1})-NaCl 0.9 wt %-water	7.4			6.8 ± 0.3	292 ± 124				42 ± 8
$(C18)_2$DTPAGlu(Gd) (0.00032 mol kg^{-1})-$(C18)_2$L5CCK8 (0.00015 mol kg^{-1})-water	4.5			4.6 ± 0.3	429 ± 26				44 ± 6
$(C18)_2$DTPAGlu(Gd) (0.00032 mol kg^{-1})-$(C18)_2$L5CCK8 (0.00016 mol kg^{-1})-water	3			2.9 ± 0.2	669 ± 40				44 ± 9

Diffusion coefficients (D) and hydrodynamic radii (R_H) obtained by DLS measurements. The terms fast and slow refer to micelles and bilayer structures, respectively. Number of aggregation (N*agg*), radius (R) and length (l) of the micelles, and thickness (d) of the bilayer structures obtained by SANS measurements.

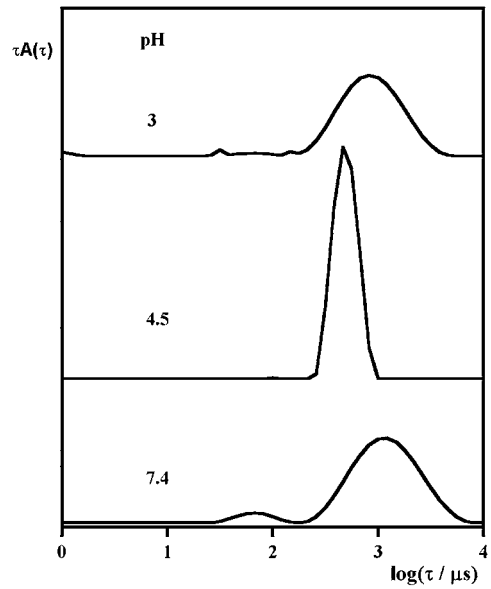

FIGURE 3 Relaxation-time distributions at $\theta = 90°$ for $(C18)_2$DTPAGlu(Gd)-$(C18)_2$L5CCK8 solution as a function of pH.

an aggregate, probably a bilayer structure, with apparent translational diffusion coefficient $D = (6.8 \pm 0.3) \times 10^{-12}$ m^2/s and an apparent hydrodynamic radius $R_H = 292 \pm 124$ Å.

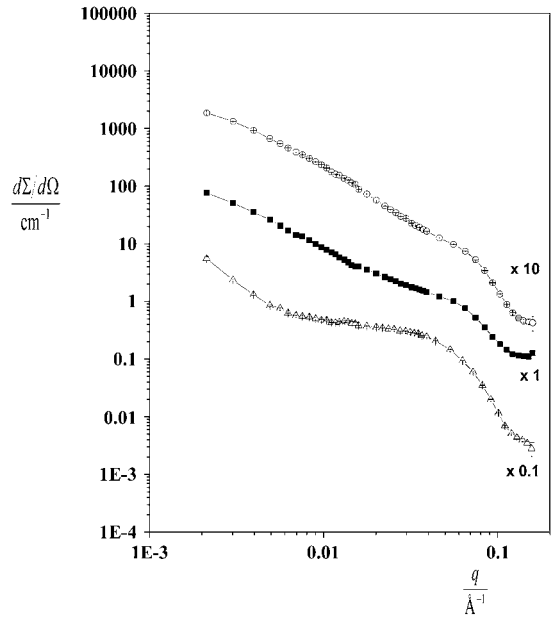

FIGURE 4 Scattering intensity profile for the following mixed systems at pH 7.4 at different molar ratios: $(C18)_2$DTPAGlu-$(C18)_2$L5CCK8-D_2O 80:20 (△), $(C18)_2$DTPAGlu-$(C18)_2$L5CCK8-D_2O 70:30 (■), $(C18)_2$DTPAGlu-$(C18)_2$L5CCK8-D_2O 60:40 (○). Solid line represents the fitting curve to the experimental data through the model reported in the text. For a better comparison, cross sections have been multiplied for a scale factor.

SANS

SANS measurements were carried out on selected samples according to DLS results to gain structural parameters of the different aggregates.

Ternary system: $(C18)_2$DTPAGlu-$(C18)_2$L5CCK8-water

The small-angle neutron scattering data of the samples containing the mixed system $(C18)_2$DTPAGlu-$(C18)_2$L5CCK8 at different ratios are presented in Fig. 4. The common feature of all the samples analyzed is the coexistence of bilayer structures and micelles. Inspection of the figure shows that all systems exhibit a power law according to an exponent d characteristic for certain spatial arrangements of our molecules in the aggregation structure. At low q values, all samples show an exponent $d = 2$, typical of planar structures. In the intermediate q range ($0.02 < q < 0.1$ Å^{-1}), the scattering profile slope changes and a smooth decay characteristic of different-shaped micelles is observed. In most of the cases, a q^{-1} power law is present in the scattering profiles, as expected for rodlike micelles. As the amount of $(C18)_2$L5CCK8 in the aggregates is raised, the extension of the q^{-2} power law relationship increases. Because the concentration of the $(C18)_2$DTPAGlu is roughly constant in all samples, the experimental evidence reflects the increase of the bilayer structure density in the systems.

Ternary system: $(C18)_2$DTPAGlu(Gd)-$(C18)_2$L5CCK8-water

The contemporary presence of $(C18)_2$L5CCK8, which is interposed among the polar heads of the chelating agent shielding the electrostatic repulsions, and Gd^{3+}, which reduces the charge of the DTPAGlu moiety drastically (from -5 to -2), supports the formation of bilayer structures so that the scattering profile is dominated by a very extended range of a q^{-2} power law, though a rising peak at $q = 0.06$ Å is present, as seen in Fig. 5 (*open triangles*).

pH effect

pH has a drastic effect on the aggregates formed by our molecules, as revealed by the SANS results presented in Fig. 5 for $(C18)_2$DTPAGlu(Gd)-$(C18)_2$L5CCK8 samples. Both the samples at pH 4.5 and 3 (solid squares and diamonds, respectively) are characterized by an extended range of q^{-2} as for bilayer structure should be expected and no evidence of any detectable peak due to the presence of small aggregates as micelles is observed.

Ionic strength effect

To investigate the effect of the physiological ionic strength in determining the nature of the aggregates formed by our molecules, small-angle neutron scattering measurements were

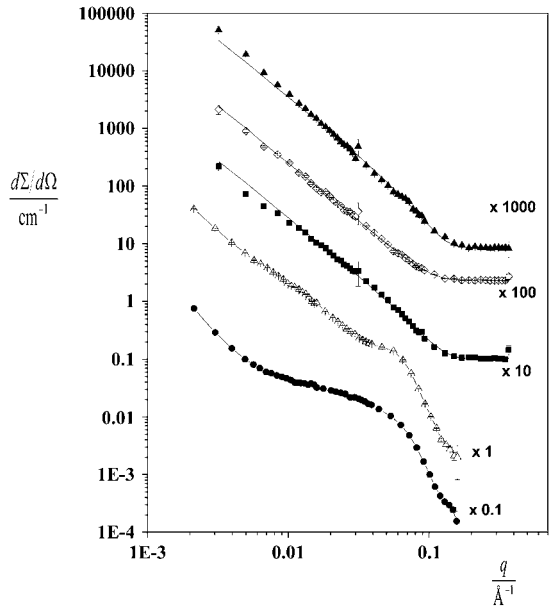

FIGURE 5 Scattering intensity profile for the following systems: $(C18)_2$DTPAGlu(Gd)-D_2O at pH 7.4 (●), $(C18)_2$DTPAGlu(Gd)-$(C18)_2$L5CCK8-D_2O at pH 7.4 (△), $(C18)_2$DTPAGlu(Gd)-$(C18)_2$L5CCK8-D_2O at pH 4.5 (■), $(C18)_2$DTPAGlu(Gd)-$(C18)_2$L5CCK8-D_2O at pH 3 (◇), $(C18)_2$DTPAGlu(Gd)-$(C18)_2$L5CCK8-D_2O at pH 7.4 in the presence of NaCl 0.9 wt % (▲). The solid line represents the fitting curve to the experimental data through the model reported in the text. For a better comparison, cross sections have been multiplied for a scale factor.

performed on the $(C18)_2$DTPAGlu(Gd)-$(C18)_2$L5CCK8 system in the presence of 0.9 wt % of NaCl. The experimental data, $I(q)$ vs. q, presented in Fig. 5 show that at physiological conditions, evidence of micelle presence disappears and bilayer structures are the only species present, in fact in quite a large q range, $I(q)$ shows a q^{-2} decay (*solid triangles*).

Cryo-TEM

Cryo-TEM images were collected only on systems in which the DTPAGlu derivative complexes the gadolinium ion, in conditions of different pH and physiological ionic strength, since these are the most interesting aggregates in the scope of the research presented here. At pH 7.4, images were dominated by the presence of elongated micelles, which appear as fibers, and planar symmetric bilayers. The latter appear as stiff tubular molecular arrangements~150 nanometers long (Fig. 6 *a*). The images reveal that these bilayer structures tend to crowd together, forming a sort of texture with an asymmetric geometry. When pH is lowered, as shown by scattering techniques, the tendency to form bilayer structures increases. At pH 3, the images were characterized by the presence of planar bilayers coexisting with vesicles with a diameter of ~120 nm (Fig. 6 *b*). The images collected in the presence of sodium chloride show a higher number of bilayer structures compared with the system at pH 7.4, in the absence of salt; Fig. 7 shows a vesicle surrounded by fibers.

DISCUSSION

Analysis of the data collected in the Results section allows a number of interesting observations regarding the system presented in this work.

The two monomers studied coaggregate, forming mixed aggregates, and thus diffuse together, as indicated by PGSE-NMR measurements. At pH 7.4, they form essentially elongated micelles. Furthermore, both the DLS and SANS results reveal the coexistence in solution of two different aggregates: micelles with an elongated shape and bilayer structures. Similar results have also been found for the $(C18)_2$DTPA-Glu-water binary system (15). However, with respect to the latter, in mixed aggregates the presence of the peptide unimer favors the formation of bilayer structures, as indicated by the magnitude of the relaxation-time distribution, which in the same conditions (total concentration, pH) appears noticeably larger than that found in the pure $(C18)_2$DTPAGlu binary system. The presence of uncharged peptide unimer that interposes between the charged headgroups of the chelating agent unimer, decreasing the strong headgroup-headgroup

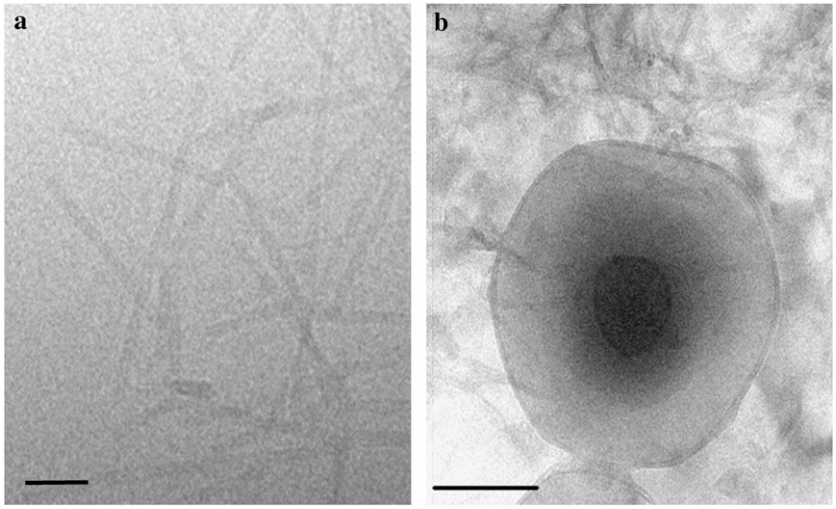

FIGURE 6 Selected cryo-TEM images for $(C18)_2$DTPAGlu(Gd)-$(C18)_2$L5CCK8 at different pH conditions. (*a*) pH 7.4, sandwiched bilayer structures. (*b*) pH 3, enlargement of the image of a vesicle. Scale bar, 50 nm.

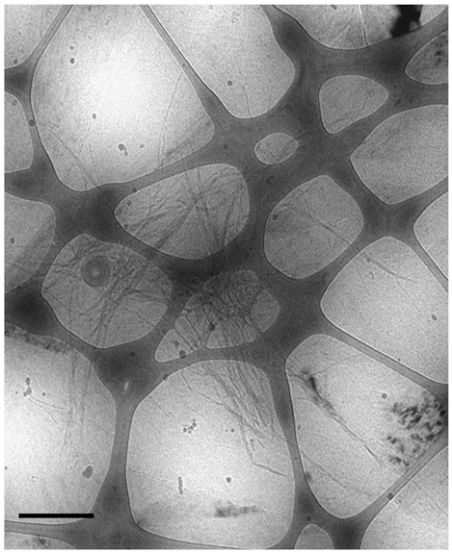

FIGURE 7 Cryo-TEM image for $(C18)_2$DTPAGlu(Gd)-$(C18)_2$L5CCK8 in the presence of NaCl 0.9 wt %. Scale bar, 0.5 μm.

electrostatic repulsions, probably supports the formation of large aggregates with a low radius of curvature. In other words, the addition of uncharged molecules in the $(C18)_2$DTPAGlu aggregates promotes a transition from small aggregates, such as micelles, to larger-size structures such as lamellar aggregates or vesicles. The transition appears to be smooth and there are not clear break points indicative of an abrupt transition. This is clearly shown by SANS results, where, upon raising the amount of $(C18)_2$L5CCK8 in the aggregates, the extension of the q^{-2} increases (see Fig. 4). Furthermore, due to the uncharged unimer insertion, the lamellar aggregates reach a size of the order of 1000 Å, as suggested by the flattening of the scattering intensity at low q ($\sim$0.005 Å^{-1}) (Fig. 4, *circles*).

The complexation of DTPAGlu with the paramagnetic Gd^{3+} ion decreases strongly the actual charge of the headgroup of the surfactant, and consequently also the high electrostatic repulsions between the different headgroups, favoring in turn the formation of lamellar aggregates. This is observed from the DLS results: the slow relaxation mode becomes slower when Gd^{3+} is present than in its absence (Fig. 3). This is in agreement with the SANS results, where a scattering profile with a power law of q^{-2} spans a larger q range (Fig. 5). However, we note that in this system also a certain number of micelles are present.

From a structural point of view, the radius and the length of these micelles are similar to those observed in the system containing DTPAGlu unimer in uncomplexed form (Table 2). The thickness of the lamellar aggregate containing gadolinium ion decreases from 70 to 50 Å, suggesting a better packing of the molecules in the double layer due to the decrease of the electrostatic repulsions. The extracted structural parameters allow us to deduce a possible picture of the aggregates formed by our molecules and thus to evaluate the effect of the spacer length on the surface of the aggregates, which was one of the aims of this work.

As mentioned, the dimension of the PEG coil is crucial in determining the shape of the aggregates and guaranteeing an efficient exposure of the peptide. In Fig. 8, we present a schematic picture of the organization of the two monomers on the surface of the aggregates based on the structural parameters evaluated by SANS fitting. In particular, according to our experimental evidence, the molecule containing the CCK8 was allocated in the aggregate with the oxyethylen glycol spacer extended through the outer shell beyond the surface of the aggregates. The part of the spacer in the hydrophilic shell was assumed to be in its extended form (4–5 oxyethylene units, for a length of $\sim$15 Å), whereas the part exposed beyond was supposed to be in its random coil configuration. In a previous article, Paduano and co-workers (22) assumed the hydrodynamic radius of this part to be equal to that obtained from the Stokes-Einstein equation applied to diffusion coefficients measured on the oxyethylene glycol series . As shown in Fig. 8, for a mixed sample (70:30 molar ratio), the size of the oxyethylene glycol units cover $\sim$20% of the surface of the aggregates and the peptide moieties are quite separated and well exposed ($\sim$15 Å beyond the aggregate surface). We note that Johnsson has evaluated the extension of oxyethylene units present on self-assembled amphiphilic molecule using a more precise method proposed by Vagberg (16). The value presented by Johnsson for an oxyethylene oligomer consisting of 10 units, such as that used here, is in agreement with what we have estimated, as described above.

The effect of the structural dependence of the $(C18)_2$DTPA-GluGd-$(C18)_2$L5CCK8 aggregate on environmental conditions such as pH and ionic strength has also been studied.

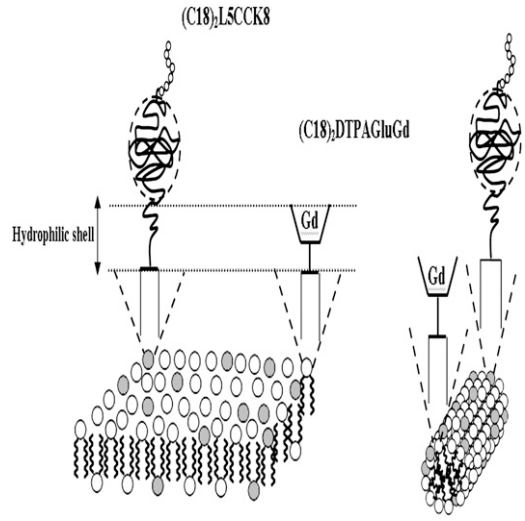

FIGURE 8 Schematic picture of the aggregates formed by our molecules according to SANS results.

Particular emphasis has been given to the pH aggregation behavior dependence, since pH-sensitive contrast agents represent a new attractive class of contrast agents in MRI. The pH effect on the aggregation state depends on the presence of carboxylic groups in the chelating agent unimer. The protonation of these carboxylic groups results in a decreased electrostatic repulsion between the headgroups. In fact decreasing pH leads to the formation of larger aggregates, such as lamellar structures, that are further favored by the presence of uncharged $(C18)_2$L5CCK8. In fact, previous investigations have shown that in the absence of $(C18)_2$L5CCK8 the $(C18)_2$DTPAGlu (as free base or as Gd^{3+} complex) at pH 4.5 forms both vesicles and micelles (15); in contrast, when $(C18)_2$L5CCK8 is incorporated in the aggregates the micelles disappear in the system.

The ionic strength has an effect similar to that of pH. The dynamic light-scattering experiments showed that the relaxation time distribution changes from bimodal to monomodal at higher ionic strength. The neutron scattering measurements indicated a similar change upon increasing ionic strength and presented a scattering profile that was nearly the same as that observed for the same system at pH 3, where the system contains only bilayer structures, as discussed above (see Fig. 5).

As previously reported, relaxivity measurements performed on the system at pH 7.4 in the absence and presence of salt have shown interesting results: r_{1p}= 18.6 and r_1= 21.0 (at 20 MHz and 25°C), respectively (17). These values are among the highest ever reported in literature for supramolecular contrast agents in MRI (23).

CONCLUSIONS

In this article, we have reported the upgrade of an amphiphilic supramolecular system with potential application as a tumor-specific contrast agent in MRI. The increased efficiency of the system, with respect to previous aggregates formed only by a molecule complexing gadolinium, is due to the presence of a second molecule containing CCK8, a peptide able to recognize tumor cells. The simultaneous presence in the aggregates of these two molecules allows the ratio between the two active principles to be tuned to achieve a balance between the need for a high enough number of metal ions complexed to show high relaxivity values and the need for a satisfactory number of well-exposed bioactive peptides.

The aggregation behavior of mixed aggregates formed by the two molecules, with the DTPAGlu-containing unimer with the chelating agent as free base or as a gadolinium complex, has been studied by means of different techniques. In both cases, scattering techniques have revealed the presence in solution of micelles and bilayer structures. The formation of the latter is favored when the paramagnetic Gd^{3+} ion is complexed, because of the decrease of the actual charge of the headgroup of the chelating-agent unimer. The aggregation properties of the $(C18)_2$DTPAGlu(Gd)-$(C18)_2$L5CCK8-water ternary system have been investigated in a wide range of pH, from 7.4 to 3, and in conditions of physiological ionic strength. When the pH is lowered or an electrolyte such as sodium chloride is added, the intra- and interaggregate electrostatic repulsions are screened, leading to the condition where bilayer structures are the dominant aggregates in solution, as confirmed by cryo-TEM images.

Relaxivity measurements carried out on the systems investigated have produced interesting values (17). Furthermore, the pH-dependent aggregation behavior contributes interesting properties to the system as a pH-sensitive contrast agent in MRI. To our knowledge, this is the first description of supramolecular aggregates with these appealing features. Such aggregates show great potential for further development in clinical use.

APPENDIX: DATA ANALYSIS

DLS

In a DLS experiment, the time (auto or pseudocross) correlation function of the scattered intensity $G^{(2)}(t)$ is measured (24). The normalized intensity correlation function $g^{(2)}(t)$ is related to the normalized time correlation function of the electric field, $[g^{(1)}(t)]$, by Siegert's relation: (25,26)

$$g^{(2)}(t) - 1 = \beta |g^{(1)}(t)|^2, \tag{4}$$

where β ($\leq$1) is a nonideality factor that accounts for deviation from ideal correlation and depends on the experimental geometry.

$g^{(1)}(t)$ can either be a single-exponential or multiexponential decay with corresponding relaxation times, τ, depending on the system investigated. It can be written as the Laplace transform of the distribution of relaxation times, $A(\tau)$:

$$g^{(1)}(t) = \int_{-\infty}^{+\infty} \tau A(\tau) \exp\left(-\frac{t}{\tau}\right) d\ln\tau. \tag{5}$$

The relaxation time distribution is obtained by regularized inverse Laplace transformation of the measured intensity correlation function using calculation algorithm REPES (25,26), as incorporated in the GENDIST analysis package (26–28). The distributions are presented as $\tau A(\tau$ versus $\log(\tau/\mu s)$.

The relaxation rate Γ ($1/\tau$) is obtained from the first moment of the relaxation time distribution, from which the apparent collective diffusion coefficient D of a translational motion can be estimated in the limit of small scattering vectors:

$$D = \lim_{q \to 0} \frac{\Gamma}{q^2}, \tag{6}$$

where q is the absolute value of the scattering vector ($q = 4\pi n_0 \sin(\theta/2)/\lambda$), where n_0 is the refractive index of the solvent, λ is the incident wavelength, and θ is the scattering angle. Thus, D can be obtained from the slope of Γ as a function of q^2, where Γ is measured at different scattering angles.

SANS

The general scattering cross section contains information about shape, size, and interactions of scattering bodies. Since the analyzed solutions are quite dilute ($c < 10^{-3}$ mol kg^{-1}), the structure function $S(q)$ can be approximated to the unity, and the scattering cross section is reduced to

$$\frac{d\Sigma}{d\Omega}(q) = n_p P(q) + \left(\frac{d\sigma}{d\Omega}\right)_{\text{inch}}, \tag{7}$$

where $P(q)$ is the form factor and contains information on the shape of the scattering objects, n_p is the number density of scattering bodies, and $(d\Sigma/d\Omega)_{inc.}$ is the incoherent scattering cross section.

Microstructural parameters of the aggregates were obtained by applying the appropriate model to the experimental SANS data. Indeed, in the analyzed systems, experimental data show the existence of cylindrical micelles and/or the presence of vesicular aggregates.

Scattering from cylindrical structures is characterized by a region where the $d\Sigma/d\Omega \approx q^{-1}$ power law dependence holds. The single-particle form factor for such micelles can be written as (29)

$$P(q) = (\rho_c - \rho_0)^2 \pi R^2 l \times \int_0^{\pi/2} \frac{\sin^2\left(q\frac{l}{2}\cos\phi\right)}{\left(q\frac{l}{2}\cos\phi\right)^2} \frac{4[J_1(qR\sin\phi)]^2}{(qR\sin\phi)^2} \sin\phi d\phi, \quad (8)$$

where l is the length of the cylinders, R the radius of the base, J_1 the first-order Bessel function, and $\rho_c - \rho_0$ the scattering-length density difference between the cylinders and the solvent.

Vesicular aggregates cannot be observed in their complete form since the Guinier region of such objects falls almost completely in the USANS domain. As a consequence, the SANS region is characterized by a power law $d\Sigma/d\Omega \approx q^{-2}$ due to the scattering of the vesicular double layer. Indeed, the q range spanned by the SANS measurements allows us to view the vesicles as randomly oriented planar sheets for which the form factor can be expressed by (30)

$$P(q) = 2\pi(\rho_c - \rho_0)^2 S d^2 \frac{1}{q^2} \frac{\sin^2\left(\frac{qd}{2}\right)}{\left(\frac{qd}{2}\right)^2}, \quad (9)$$

where d is the plane thickness and S is the plane surface per unit volume.

Scattering from solutions containing cylindrical structures has been analyzed using Eqs. 7 and 8, whereas in the systems containing vesicular aggregates, Eqs. 7 and 9 were used. For systems containing both objects, we assumed that each kind of aggregate scattered independently from the other, expressed the cross section as the sum of the form factors weighted for two scale factors (K_{cyl}, K_{sheets}) the relative number density of the object

$$\frac{d\Sigma}{d\Omega}(q) = n_p K_{cyl} P_{cyl}(q) + K_{sheets} P_{sheets}(q) + \left(\frac{d\sigma}{d\Omega}\right)_{inch}, \quad (10)$$

and treated the scale factors as adjustable parameters.

By fitting the appropriate model to the experimental data, it was possible to extract the radius R of the cylinders and the thickness d of the sheets.

The length of the cylinders cannot always be extracted from the scattering data in the accessible range of the scattering vector q ($q > 0.002 Å^{-1}$), as indicated by the absence of the Guinier region at low q. As a result of that, in the tables, large numbers are taken as the lower limit for the real length.

The authors are grateful to Gunnel Karlsson for the cryo-TEM imaging. M.V., G.M., and L.P. wish to thank the Forschungszentrum Jülich and the Hahn Meitner institut for providing beam time. The authors thank Dr. Eliana Gianolio for relaxivity measurements.

SANS experiments were supported by the European Commission, NMI3 ContractRII3-CT-2003-505925. The authors thank the European Molecular Imaging Laboratories Network (EMIL) for financial support.

REFERENCES

1. Aime, S., M. Botta, M. Fasano, and E. Terreno. 1998. Lanthanide (III) chelates for NMR biomedical applications. *Chem. Soc. Rev.* 27:19–29.
2. Laus, S., A. Sour, R. Ruloff, E. Toth, and A. E. Merbach. 2005. Rotational dynamics account for pH-dependent relaxivities of PA-MAM dendrimeric, Gd-based potential MRI contrast agents. *Chem. Eur. J.* 11:3064–3076.
3. Nakamura, E., K. Makino, T. Okano, T. Yamamoto, and M. Yokoyama. 2006. A polymeric micelle MRI contrast agent with changeable relaxivity. *J. Controlled Release.* 114:325–333.
4. Dirksen, A., S. Langereis, B. F. M. de Waal, M. H. P. van Genderen, T. M. M. Hackeng, and E. W. Meijer. 2005. A supramolecular approach to multivalent target-specific MRI contrast agents for angiogenesis. *Chem. Commun.*2811–2813.
5. Toth, E. B., R. D. Bolskar, A. Borel, G. Gonzalez, L. Helm, A. E. Merbach, B. W. Sitharaman, and L. J. Wilson. 2005. Water-soluble gadofullerenes: toward high relaxivity, pH-responsive MRI contrast agents. *J. Am. Chem. Soc.* 127:799–805.
6. Accardo, A., D. Tesauro, P. Roscigno, E. Gianolio, L. Paduano, G. D'Errico, C. Pedone, and G. Morelli. 2004. Physicochemical properties of mixed micellar aggregates containing CCK peptides and Gd complexes designed as tumor specific contrast agents in MRI. *J. Am. Chem. Soc.* 126:3097–3107.
7. Gløgård, C., G. Stensrud, R. Hovland, S. L. Fossheim, and J. Klaveness. 2002. Liposomes as carriers of amphiphilic gadolinium chelates: the effect of membrane composition on incorporation efficacy and in vitro relaxivity. *Int. J. Pharm.* 233:131–140.
8. Brechbiel, M. W., R. A. Star, and H. Kobayashi. 2004. Dendrimer-based nanosized MRI contrast agents. U. S. Pat. Appl. Publ. 2004037777.
9. Mikawa, M., N. Miwa, M. Brautigam, T. Akaike, and A. Maruyama. 2000. Gd^{3+}-loaded polyion complex for pH depiction with magnetic resonance imaging. *J. Biomed. Mater. Res.* 49:390–395.
10. Louie, A. Y., M. M. Hüber, E. T. Ahrens, U. Rothbächer, R. Moats, R. E. Jacobs, S. E. Fraser, and T. J. Meade. 2000.In vivo visualization of gene expression using magnetic resonance imaging. *Nat. Biotechnol.* 18:321–325.
11. Anelli, P. L., F. Fedeli, O. Gazzotti, L. Lattuada, G. Lux, and F. Rebasti. 1999. L-glutamic acid and L-lysine as useful building blocks for the preparation of bifunctional DTPA-like ligands. *Bioconjug. Chem.* 10:137–140.
12. Silvente-Poirot, S., M. Defresne, N. Vaysse, and D. Fourmy. 1993. The peripheral cholecystokinin receptors. *Eur. J. Biochem.* 215:513–529.
13. Wank, S. A. 1995. Cholecystokinin receptors. *Am. J. Physiol.* 269:628–646.
14. Reubi, J. C., J. C. Schaer, and B. Waser. 1997. Cholecystokinin(CCK)-A and CCK-B/gastrin receptors in human tumors. *Cancer Res.* 57:1377–1386.
15. Vaccaro, M., A. Accardo, D. Tesauro, G. Mangiapia, D. Löf, K. Schillén, O. Söderman, G. Morelli, and L. Paduano. 2006. Supramolecular aggregates of amphiphilic gadolinium complexes as blood pool MRI/MRA contrast agents: physicochemical characterization. *Langmuir.* 22:6635–6643.
16. Johnsson, M., P. Hansson, and K. Edwards. 2001. Spherical micelles and other self-assembled structures in dilute aqueous mixtures of poly(ethylene glycol) lipids. *J. Phys. Chem. B.* 105:8420–8430.
17. Accardo, A., D. Tesauro, G. Morelli, E. Gianolio, S. Aime, M. Vaccaro, G. Mangiapia, L. Paduano, and K. Schillén. 2007. High-relaxivity supramolecular aggregates containing peptides and Gd complexes as contrast agents in MRI. *J. Biol. Inorg. Chem.* 12:267–276.
18. Johnson, C. S. 1999. Diffusion ordered nuclear magnetic resonance spectroscopy: principles and applications. *Prog. Nucl. Magn. Reson. Spectrosc.* 34:203–256.
19. Jansson, J., K. Schillén, G. Olofsson, R. Cardoso da Silva, and W. J. Loh. 2004. The interaction between PEO-PPO-PEO triblock copolymers and ionic surfactants in aqueous solution studied using light scattering and calorimetry. *J. Phys. Chem. B.* 108:82–92.
20. Bellare, J. R., H. T. Davis, L. E. Scrivan, and Y. J. Talmon. 1988. Controlled environment vitrification system: an improved sample preparation technique. *J. Electron Microsc. Tech.* 10:87–111.
21. Jonstromer, M., B. Johnsson, and B. Lindman. 1991. Self-diffusion in nonionic surfactant-water systems. *J. Phys. Chem.* 95:3293–3300.
22. Vergara, A., L. Paduano, V. Vitagliano, and R. Sartorio. 1999. Mutual diffusion in aqueous solution of poly(ethyleneglycol) samples. Some

comments on the effect of chain length and polydispersity. *Phys. Chem. Chem. Phys.* 23:5377–5383.

23. Mulder, W. J. M., G. J. Strijkers, G. A. F. van Tilborg, A. W. Griffioen, and K. Nicolay. 2006. Lipid-based nanoparticles for contrast-enhanced MRI and molecular imaging. *NMR Biomed.* 19:142–164.
24. Berne, B. J., and R. Pecora. 2000. Dynamic Light Scattering: With Applications to Chemistry, Biology and Physics. Dover Publications, Mineola, NY.
25. Siegert, A. J. F. 1943. On the fluctuations in signals returned by many independent scatterers. Report No. 465. MIT Radiation Laboratory. Available at: http://ieeexplore.ieee.org/ie15/18/22674/01055132.pdf?tp=&isnumber=arnumber=1055132.
26. Stepánek, P. 1993. Data analysis in dynamic light scattering. *In* Dynamic Light Scattering: The Method and Some Applications. W. Brown, editor. Oxford University Press, Oxford, UK.
27. Johnsen, R., W. Brown, S. E. Harding, D. B. Sattelle, and V. A. Bloomfield. 1992. Laser Light Scattering in Biochemistry. Royal Society of Chemistry, Cambridge, UK.
28. Schillén, K., W. Brown, and R. Johnsen. 1994. Micellar sphere-to-rod transition in an aqueous triblock copolymer system. A dynamic light scattering study of translational and rotational diffusion. 1994. *Macromolecules.* 27:4825–4832.
29. Kotlarchyk, M., and S. H. Chen. 1983. Analysis of small angle neutron scattering spectra from polydisperse interacting colloids. *J. Chem. Phys.* 79:2461–2469.
30. Ma, G., D. J. Barlow, M. J. Lawrence, R. K. Heenan, and P. Timmins. 2000. Small-angle neutron-scattering studies of nonionic surfactant vesicles. *J. Phys. Chem. B.* 104:9081–9085.